

MODELING AND OPTIMIZATION OF CUTTING PARAMETERS WHEN TURNING EN-AW-1350 ALUMINUM ALLOY

F. KHROUF*

Laboratory of Mechanics, Chaabet-Ersas Campus, Mechanical Eng. Dept.,
Université Frères Mentouri, 25000 Constantine -1, ALGERIA
E-mail: fakhreddine.khrouf@umc.edu.dz

H.TEBASSI and M.A. YALLESE

Mechanics and Structures Research Laboratory (LMS), Mechanical Eng. Dept.,
Université 8 Mai 1945 Guelma, BP 401, 24000 Guelma, ALGERIA

K. CHAOUI

Mechanics of Materials and Industrial Maintenance Research Laboratory (LR3MI),
Mechanical Eng. Dept., Badji Mokhtar University, PO Box 12, 23052 Annaba, ALGERIA

A. HADDAD

Applied Mechanics for New Materials Laboratory (LMANM), Mechanical Eng. Dept.,
Université 8 Mai 1945 Guelma, BP 401, 24000 Guelma, ALGERIA

An experimental investigation is carried out to examine the effects of various cutting parameters on the response criteria when turning EN-AW-1350 aluminum alloy under dry cutting conditions. The experiments related to the analysis of the influence of turning parameters on the surface roughness (Ra) and material removal rate (MRR) were carried out according to the Taguchi L27 orthogonal array (3^{13}) approach. The analysis of variance (ANOVA) was applied to characterizing the main elements affecting response parameters. Finally, the desirability function (DP) was applied for a bi-objective optimization of the machining parameters with the objective of achieving a better surface finish (Ra) and a higher productivity (MRR). The results showed that the cutting speed is the most dominant factor affecting Ra followed by the feed rate and the depth of cut. Moreover, the Artificial Neural Network (ANN) approach is found to be more reliable and accurate than its Response Surface methodology (RSM) counterpart in terms of predicting and detecting the non-linearity of the surface roughness and material removal rate mathematical models. ANN provided prediction models with a precision benefit of 8.21% more than those determined by RSM . The latter is easier to use, and provides more information than ANN in terms of the impacts and contributions of the model terms.

Key words: ANOVA, Artificial Neural Networks, chip shape, optimization, response surface methodology.

1. Introduction

The excellent machinability characteristics of aluminum alloys match perfectly the modern machining techniques that mostly depend on reliable processes and increased productivity as these are necessary for the reduction of costs and the improvement of competitiveness. Machinability may be defined as the relative difficulty presented by a material during its machining. Its value is mainly determined by five parameters: the surface roughness, the cutting forces, the tool life, the chip formation and the flank wear [1-4]. Models for the cutting operation can be developed using classical approaches such as linear and quadratic regression or artificial intelligence methods. The latter techniques use unconventional approaches such as

* To whom correspondence should be addressed

Artificial Neural Networks (ANN), Fuzzy Logic (FL) and Genetic Algorithms (GA). Several research works have investigated and applied these techniques. Rafael F. Garcia *et al.* [5] experimentally investigated the influence of machining conditions represented by the cutting parameters (V_c , f and a_p) along with the dry and reduced quantity lubricant conditions on the surface roughness (R_a and R_z) in turning of 6082-T6 aluminum alloy using uncoated carbide tool. Through the application of Box–Behnken design, they succeeded in establishing a correlation between the friction conditions and the surface roughness. Their results indicate that the feed rate is the most significant input variable on the R_a and R_z mean values among those analyzed (V_c , f , a_p) for both dry and reduced quantity lubricant machining.

Rajesh Kumar Bhusha [6] carried out statistical modeling using the *RSM* method in order to investigate the effect of the four process parameters (cutting speed, feed rate, depth of cut and nose radius) on the surface roughness and tool wear in CNC turning of AA7075/SiC composites. They concluded that the depth of cut and tool nose radius were main factors affecting surface roughness, and that the abrasive wear of the tungsten carbide rises when the nose radius increases. This reduces tool life. Seyed Hasan Musavi *et al.* [7] carried out a statistical analysis using the Response Surface Methodology (*RSM*) in order to derive the machining response represented by the surface roughness and tool wear in the turning of 7075 aluminum alloy with a cemented uncoated carbide insert. They concluded that the *RSM* combined with a factorial design of the experiments represent a useful technique for the surface roughness and tool wear evaluation, and that the tool wear and surface roughness results for MQL machining were better than those recorded under dry mode. This phenomenon can be attributed to a better transfer of cutting fluid particles to the machining area in the MQL method.

An aluminum alloy has a low density, high strength, good fracture toughness along with a high stress corrosion resistance. It is thus an ideal light structure material for use in applications related to aerospace, manufacturing, automotive and aeronautics industries [8, 9]. Fang *et al.* [10] performed cutting experiments on the 2024-T351 aluminum alloy using cemented carbide inserts, and examined the effect of the built-up edge on the cutting vibrations. They found out that the most significant factors affecting the vibration amplitude were the cutting speed (53%) followed by the feed rate (33.3%). Demir and Gündüz [11] experimentally investigated the effects of aging on the machinability of 6061 aluminum alloy using CVD multi-layer coated cemented carbide inserts. Their experimental results showed that increasing cutting speed leads to decreasing surface roughness, and this has been interpreted as a result of the decreasing built-up edge formation tendency which is a consequence of the increase the cutting speed. Sahoo *et al.* [12] carried out statistical modeling using both the weighted principal component analysis and *RSM* in order to investigate the effect of the process parameters on the surface roughness and tool vibration in CNC turning of aluminum alloy 63400. They concluded that the interaction effects of the spindle speed (V_c) and feed rate (f) were significant for the model in the case of tool vibration. They were, however, insignificant in the case of the surface roughness.

In high speed CNC manufacturing process is usually adopted because of its low cost along with its increased machining accuracy. Moreover and due to thixotropy, which is a property that allows the material to be ‘work-softened’ due to the shear strain imparted on it by the tool’s cutting edge and then to revert back to its original hardness properties once the cutting operation is complete, aluminum alloys seem to be the ideal candidates for high speed cutting processes. Therefore, high productivity along with best precision and surface qualities in manufacturing can be achieved at high cutting speeds and feed rates. Surface roughness is generally a consequence of the process parameters represented by the cutting conditions (depth of cut, feed rate, and cutting speed), the tool geometry (nose radius, inclination angle, and rake angle) and the tool material [13-15].

In the last two decades, the artificial neural network (ANN) has come up as one of the most efficient methods for empirical modeling, especially for non-linear processes as well as modeling of output parameters in machining. With that in mind, Das *et al.* [16] justified the use of artificial neural network to develop relationships between the cutting process parameters and the surface roughness when machining Al-4.5Cu-1.5TiC metal matrix composites. Moreover, Palavar *et al.* [17] concluded that the prediction of the aging effects on the wear behavior of Inconel 706 super alloy using the ANN can provide effective results, and that the method can be adequately used to detect weight loss values in the determined parameters with a

high coefficient of assurance value. In addition, the ANN approach can save time and reduce costs in experimental processes as it provides quicker results. Several researches discussed the capabilities and accuracies of the *RSM* and ANN approaches. In their comparative study, Tebassi *et al.* [18] concluded that ANN models are found to be capable of better predictions of surface roughness and cutting force within the range they have been applied than the *RSM* models in terms of better correlation and lower error.

In this study, the Taguchi *L27* orthogonal array (3^{13}) approach and ANN were adopted for developing a relationship between the experimental variables (cutting speed, feed rate and depth of cut) and machining process output parameters (surface roughness and material removed rate). Moreover, both approaches were compared in terms of the better coefficient of determination (R^2), lower root mean square error (*RMSE*) and mean predictive error (*MPE*). The predicted conversion using ANN and *RSM* models is discussed to determine which approach has better accuracy and capability for predicting surface roughness and material removed rate when turning *EN-AW-1350* aluminum alloy.

2. Experimental arrangement and procedure

2.1. Turning conditions and materials

Turning operations are carried out on a *CNC SPINNER-TC65* lathe that develops a maximum spindle speed of *4500 rpm* and a spindle power of *16.5/562-4500-kW* under dry conditions.

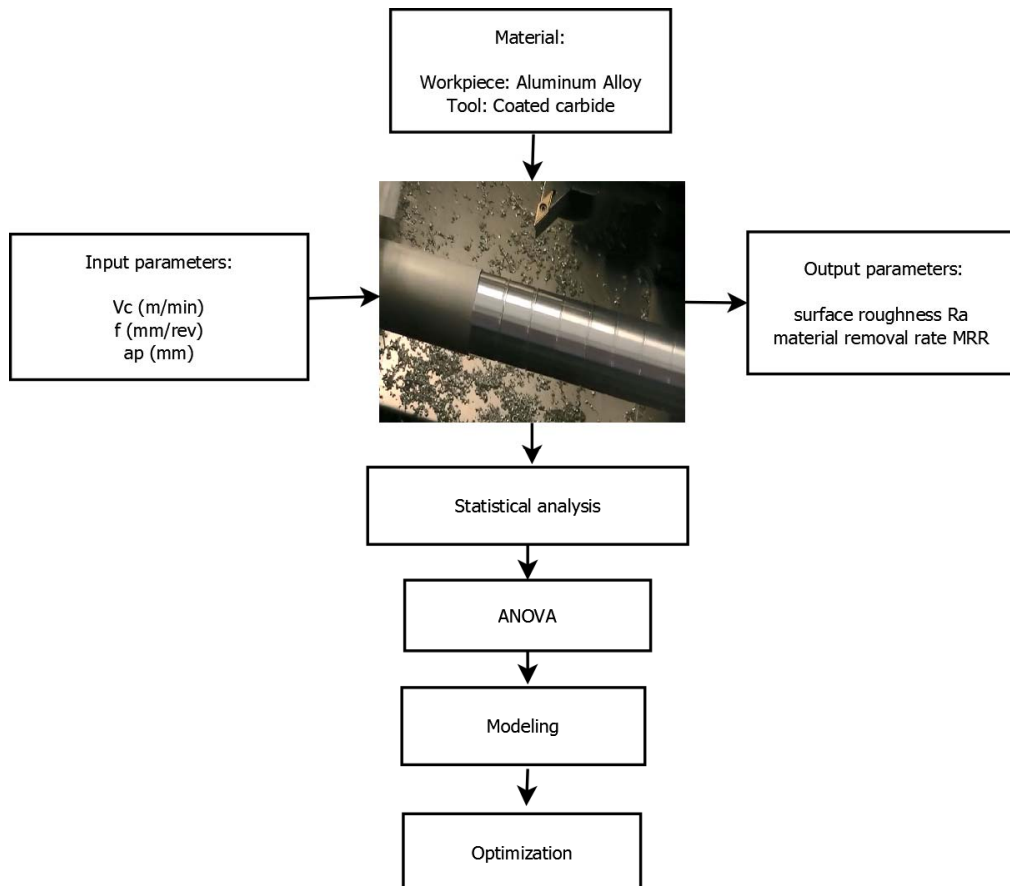


Fig.1. Schematic of experimental setup.

The measurements of arithmetic surface roughness for each cutting condition were obtained from a *PCE-RT 1200* Roughness Tester with a cut-off length of *0.8 mm* and sampling length of *4 mm*. The

measurements were repeated at five equally spaced locations around the circumference of the workpiece and the result is an average of these values for a given machining pass. Vickers hardness is evaluated using a digital micro-hardness tester *HVS-1000Z*. All tests are carried out on previously polished samples under a consistent load of *30 kgf* applied for approximately *15* seconds. A minimum of four readings are taken for each sample, and the average is derived. The hardness of the workpiece is *HV142*. The experimental setup is displayed in Fig.1.

2.2. Workpiece material and cutting tool

On the basis of their properties, lightweight aluminum alloys with high strength have been and are still adopted for various applications. The *8xxx* series are used in air-conditioning while the *7xxx* series, because of their good weldability, are needed for manufacturing of aircraft wings and in the aerospace and marine industries in general. All the remaining series (from *6xxx* to *1xxx*) are employed in a wide range of applications ranging from automotive to aerospace industries as well as architecture and packaging. Chemical composition of *EN AW 1350 aluminum alloy* is reported in Table 1. Specimens of *500mm* in length and *50 mm* in diameter are adopted for the turning process using a coated carbide tool. Cutting tools and the tool holder characteristics are given in Tab.2.

Table 1. Chemical composition of *EN AW 1350 aluminum alloy*.

Elements	Fe	Si	Cu	Zn	Cr	Ti	Mg	Mn
Composition (wt %)	<i>0.19</i>	<i>0.11</i>	<i>0.023</i>	<i>0.038</i>	<i>0.010</i>	<i>0.018</i>	<i>0.021</i>	<i>0.09</i>

Table 2. Characteristics of the cutting tool and the tool holder.

Cutting tool Type	Tool holder					
	Active zone geometry			Cutting edge length (mm)	Type	Length (mm)
principal cutting edge angle	cutting edge angle	nose radius (mm)				
VNGA	<i>93°</i>	<i>5°</i>	<i>0.4</i>	<i>16</i>	<i>SVJBL 2020 K16</i>	<i>125</i>

2.4. Organization of experiments

In order to reduce resources and time without compromising quality, the Taguchi *L27* orthogonal array (3^{13}) approach was adopted for developing a relationship between the independent input process parameters and output process responses. Consequently, the present experiments develop 27 rows corresponding to the number of parameter combinations (26 degrees of freedom) along with 13 columns at three levels.

Tests were performed according to three levels of cutting speeds (*600*, *650* and *700 m/min*), feed rates (*0.02*, *0.03* and *0.05 mm/rev*) and depths of cut (*0.2*, *0.3* and *0.4 mm*). The combination of the orthogonal array *L27* parameters along with the measured results for both the surface roughness (*Ra*) and the metal removal rate (*MRR*) are presented in Table 3. The levels of the cutting parameters are selected from the intervals recommended by the cutting tools manufacturer. The material removal rate is expressed by Eq.(2.1) as:

$$MRR(cm^3/min) = Vc \times f \times ap. \quad (2.1)$$

Table 3. Experimental data for EN AW 1350 aluminum alloy.

N°	Actual factors			Responses	
	V_c (m/min)	f (mm/rev)	a_p (mm)	R_a (μm)	MRR (cm^3/min)
1	600	0.02	0.2	0.585	2.4
2	600	0.02	0.3	0.563	3.6
3	600	0.02	0.4	0.742	4.8
4	600	0.03	0.2	0.671	3.6
5	600	0.03	0.3	0.706	5.4
6	600	0.03	0.4	0.717	7.2
7	600	0.05	0.2	1.533	6
8	600	0.05	0.3	1.747	9
9	600	0.05	0.4	1.671	12
10	650	0.02	0.2	0.456	2.6
11	650	0.02	0.3	0.671	3.9
12	650	0.02	0.4	0.683	5.2
13	650	0.03	0.2	0.517	3.9
14	650	0.03	0.3	0.572	5.85
15	650	0.03	0.4	0.609	7.8
16	650	0.05	0.2	0.662	6.5
17	650	0.05	0.3	0.714	9.75
18	650	0.05	0.4	0.729	13
19	700	0.02	0.2	0.343	2.8
20	700	0.02	0.3	0.402	4.2
21	700	0.02	0.4	0.31	5.6
22	700	0.03	0.2	0.591	4.2
23	700	0.03	0.3	0.493	6.3
24	700	0.03	0.4	0.465	8.4
25	700	0.05	0.2	0.634	7
26	700	0.05	0.3	0.61	10.5
27	700	0.05	0.4	0.64	14

3. Taguchi design based approach

3.1. Analysis of variance

In order to show the process parameters influence on the output responses, the Analysis of Variance (ANOVA) approach was applied. Tables 4 and 5 present the ANOVA results regarding the surface roughness and material removal rate, respectively. The analysis was carried out with a 5% significance level, i.e. for a confidence level of 95%. A low p-value indicates a high statistical significance of the source over its corresponding response.

From Tab.4, it can be seen that the two most important factors affecting the surface roughness are the cutting speed and the feed rate with contributions of 38.16% and 28.69%, respectively. They are followed by the cutting speed-feed rate interaction with a contribution of 15.38% while the remaining parameters did not show any significantly meaningful influence on the surface roughness (R_a). These results are in perfect agreement with many research works.

Table 4. ANOVA table for surface roughness (R_a).

Source	Sum of squares	DF	Mean	F- value	p- value	Cont. (%)	Remarks
Model *	2.89	9	0.32	11.12	< 0.0001	85.50	Significant
<i>A-Vc</i>	1.29	1	1.29	44.53	< 0.0001	38.16	Significant
<i>B-f</i>	0.97	1	0.97	33.67	< 0.0001	28.69	Significant
<i>C-ap</i>	0.017	1	0.017	0.59	0.4512	0.50	Not Significant
<i>AB</i>	0.52	1	0.52	18.00	0.0005	15.38	Significant
<i>AC</i>	0.020	1	0.020	0.70	0.4132	0.59	Not Significant
<i>BC</i>	5.171E-004	1	5.171E-004	0.018	0.8952	0.015	Not Significant
A^2	0.089	1	0.089	3.09	0.0966	2.63	Not Significant
B^2	0.047	1	0.047	1.62	0.2206	1.39	Not Significant
C^2	2.933E-003	1	2.933E-003	0.10	0.7539	0.086	Not Significant
Residual	0.49	17	0.029				
Total	3.38	26					

$R^2=0.8548, R^2$ (adjusted)=0.7779

Table 5. ANOVA table for material removal rate (MRR).

Source	Sum of squares	DF	Mean squares	F-value	p-value	Cont.(%)	Remarks
Model *	261.50	9	29.06	10584.46	< 0.0001	99.98	Significant
<i>A-Vc</i>	4.87	1	4.87	1775.61	< 0.0001	1.86	Significant
<i>B-f</i>	154.00	1	154.00	56100.46	< 0.0001	58.87	Significant
<i>C-ap</i>	91.53	1	91.53	33341.92	< 0.0001	34.99	Significant
<i>AB</i>	0.63	1	0.63	229.50	< 0.0001	0.240	Significant
<i>AC</i>	0.33	1	0.33	121.43	< 0.0001	0.126	Significant
<i>BC</i>	11.83	1	11.83	4309.50	< 0.0001	4.523	Significant
A^2	0.000	1	0.000	0.000	1.0000		Not Significant
B^2	0.000	1	0.000	0.000	1.0000		Not Significant
C^2	0.000	1	0.000	0.000	1.0000		Not Significant
Residual	0.047	17	2.745E-003				
Total	261.55	26					

$R^2=0.9998, R^2$ (adjusted)=0.9997

ANOVA results for MRR , reported in Tab.5, demonstrate that the main contribution is performed by the feed rate (58.87%) followed by the depth of cut and the cutting speed with 34.99% and 1.86%, respectively. The diverse interactions achieve contributions corresponding to 0.240%, 0.126% and 4.523% for the cutting speed-feed rate, cutting speed-depth of cut and the feed rate-depth of cut, respectively while the remaining terms influence is found insignificant. Optimum machining conditions that maximize the material removal rate are found to be $V_c=700$ m/min, $f=0.05$ mm/rev and $ap=0.4$ mm. Moreover, the highest amount of material removal rate of 14000 mm³/min is achieved at the highest feed rate and depth of cut. This agrees well with the results achieved by [19,20].

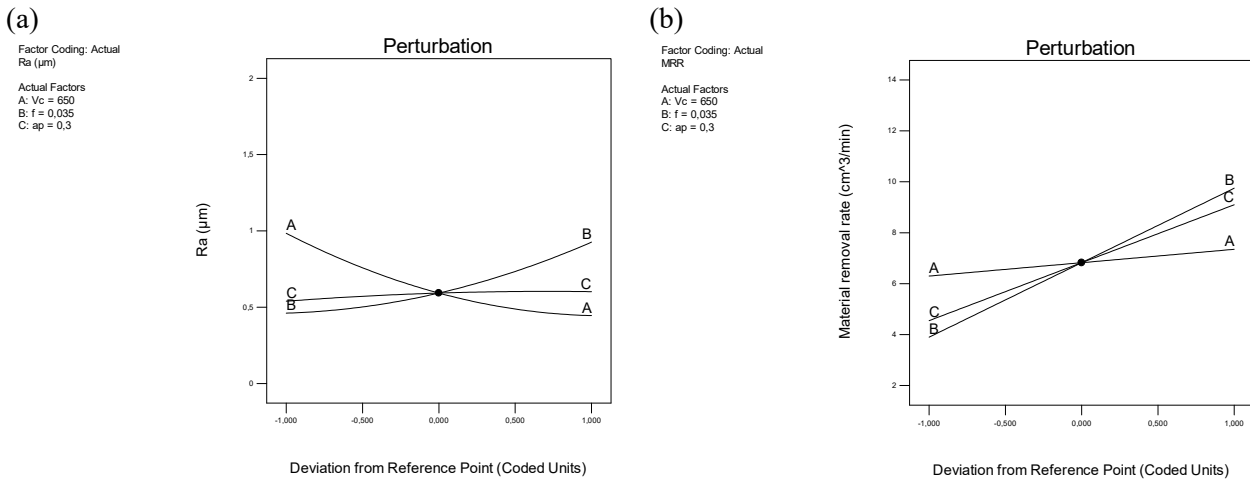


Fig.2. Perturbation plots: (a) for R_a and (b) for MRR .

3.2. Regression equations

According to the references, the correlations relating the different factors to the performance measures were modeled by quadratic regressions. The obtained equations are:

$$\begin{aligned}
 Ra = & +16.590 - 0.05685 \times V_c + 162.5305 \times f + 7.1404 \times \\
 & \times a_p - 0.2726 \times V_c \times f - 8.233 \cdot 10^{-3} \times V_c \times a_p - 4.2976 \times \\
 & \times f \times a_p + 4.8822 \cdot 10^{-5} \times V_c^2 + 449.4444 \times f^2 - 2.2111 \times a_p^2,
 \end{aligned} \quad (3.1)$$

$$\begin{aligned}
 MRR = & +6.49 - 9.999 \cdot 10^{-3} \times V_c - 195.00 \times f - 21.66 \times \\
 & \times a_p + 0.30 \times V_c \times f + 0.03 \times V_c \times a_p + 650 \times f \times a_p + \\
 & - 3.177 \cdot 10^{-18} \times V_c^2 - 6.05 \cdot 10^{-13} \times f^2 + 8.51 \cdot 10^{-14} \times a_p^2.
 \end{aligned} \quad (3.2)$$

In the present case, these models are reduced by eliminating the terms that have no significant influence on the responses. The final relationships may then be expressed as:

$$Ra = 16.590 - 0.05685 \times V_c + 162.535 \times f - 0.2726 \times V_c \times f, \quad (3.3)$$

$$\begin{aligned}
 MRR = & +6.49 - 9.999 \cdot 10^{-3} \times V_c - 195.00 \times f - 21.66 \times a_p + \\
 & + 0.30 \times V_c \times f + 0.03 \times V_c \times a_p + 650 \times f \times a_p.
 \end{aligned} \quad (3.4)$$

3.3. Surface plots

The "Design-Expert v10" software was applied for the development of the experimental plan for the RSM. Figures 3, 4 and 5 show the estimated response surface plots for (R_a) against the cutting parameters represented by the cutting speed, the feed rate and the depth of cut. It can be observed that the surface roughness (R_a) rapidly increases with the feed rate. Figure 4 clearly shows that the greatest surface roughness is achieved for a cutting speed comprised between 660 m/min and 700 m/min. Many researchers [19,20] indicate that the feed rate is one of the main factors affecting the surface roughness (R_a).

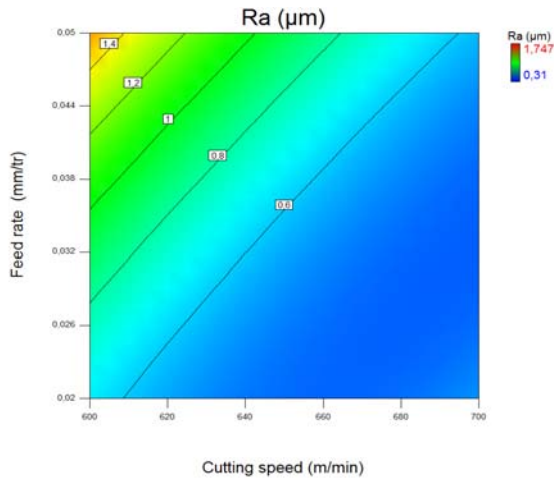


Fig.3. Contour plot for Ra vs (V_c and f).

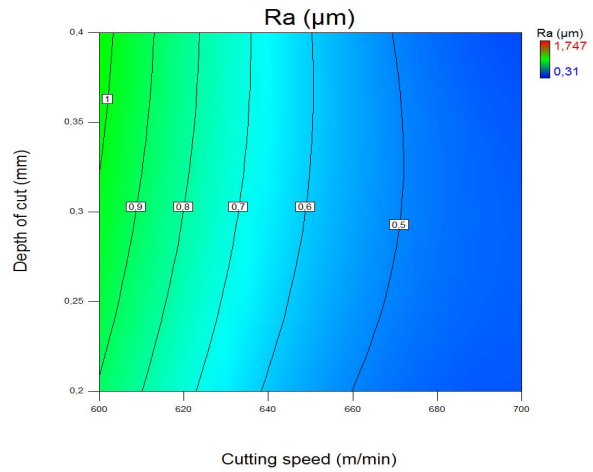


Fig.4. Contour plot for Ra vs (V_c and a_p).

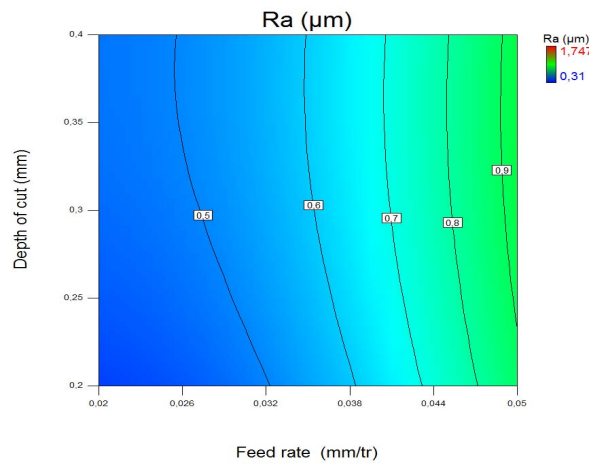


Fig.5. Contour plot for Ra vs (f and a_p).

Figures 6, 7 and 8 exhibit the estimated contour plot and response surface plots for the material removal rate (MRR) as a function of the cutting parameters represented by the cutting speed, the feed rate and the depth of cut. It can be observed the (MRR) increases with all the cutting parameters under consideration. Similar explanations have been mentioned in [19-20] regarding the effect of the cutting parameters (V_c, f, a_p) on the material removal rate (MRR).

3.4 Residual analysis

Figures 9 and 10 illustrate the residuals concerning both the surface roughness and the material removal rate models. It can be observed that the points are evenly split by a 45° line. The residuals normal probability (Figs 11 and 12) show all the residual points falling along a straight line, and that means that the errors are normally distributed. This leads to conclusion that the developed regression models for (Ra) and (MRR) are acceptable within the experimental range considered.

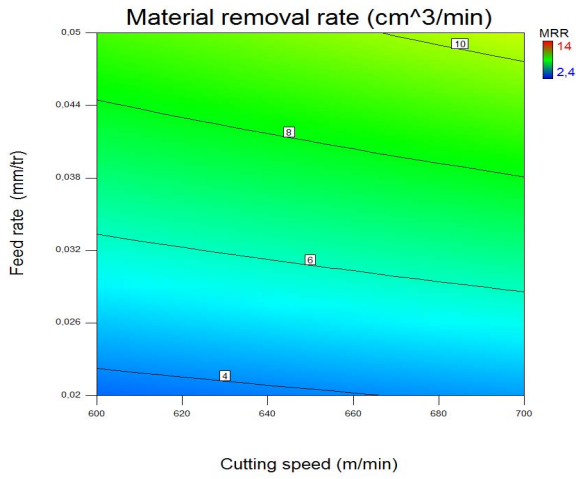


Fig.6. Contour plot for *MRR* vs (*Vc* and *f*).

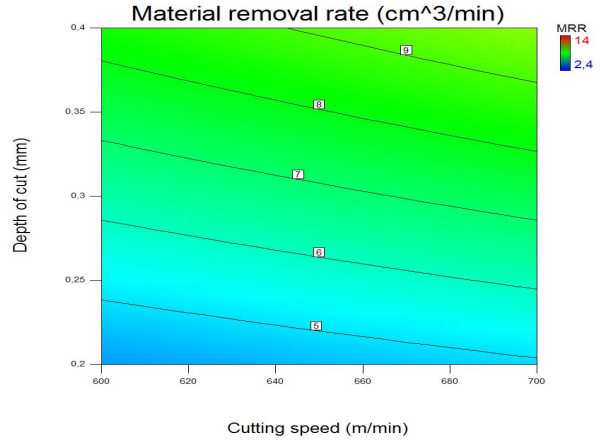


Fig.7. Contour plot for *MRR* vs (*Vc* and *ap*).

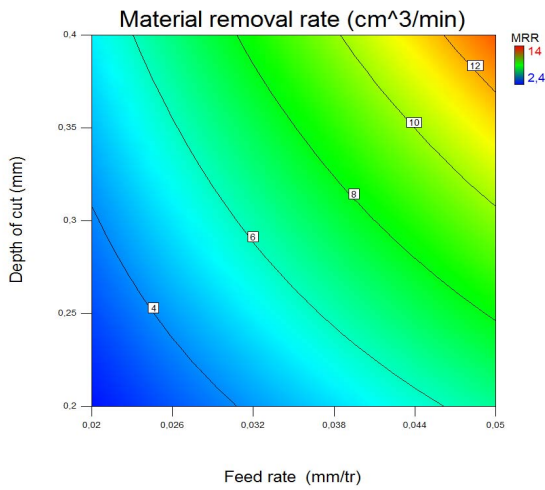


Fig.8. Contour plot for *MRR* vs (*ap* and *f*).

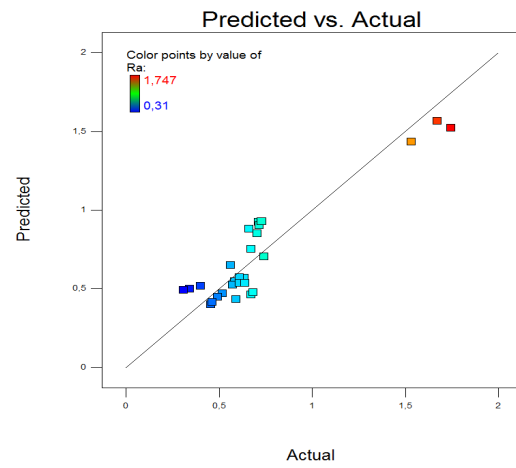


Fig.9. Predicted vs experimental residuals for *Ra*.

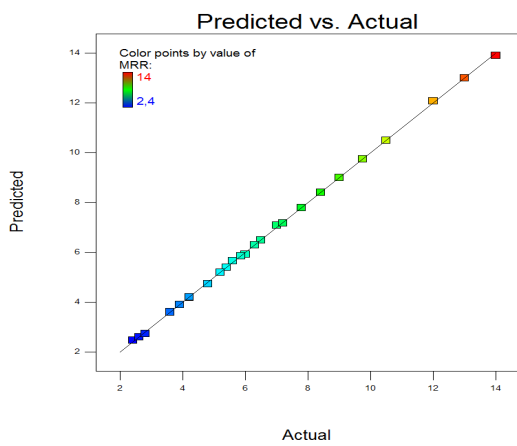


Fig.10. Predicted vs experimental residuals for *MRR*.

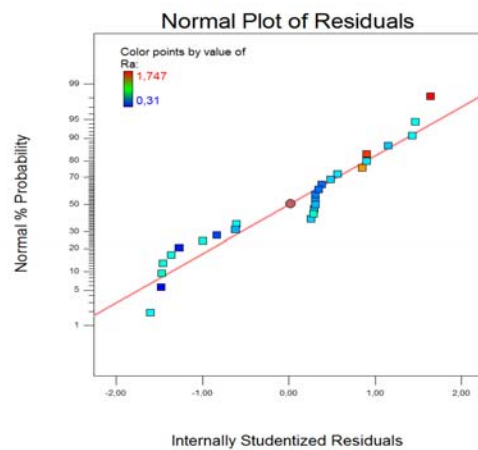


Fig.11. Normal probability residuals for *Ra*.

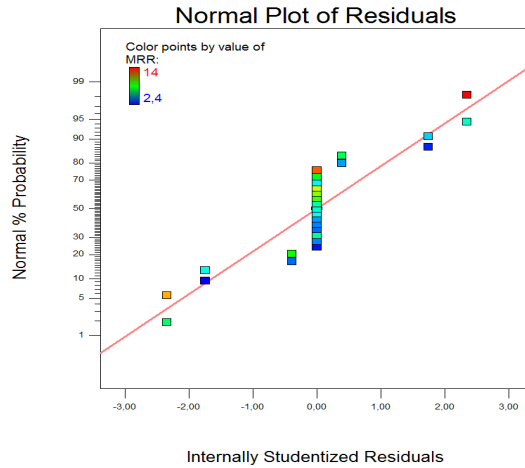


Fig.12. Normal probability residuals for *MRR*.

4. Desirability Function (*DF*) application and optimization

The desirability function method has been used in numerous research studies [21-25] in order to optimize a manufacturing process pertaining to turning, milling or various other operations [26,27]. This approach allows the combination of multiple responses into a single function (the Desirability Function or *DF*) through the choice of a value comprised between zero and one (least to most desirable, respectively). During the optimization process, the aim is to minimize the surface roughness and maximize the material removal rate. The response surface optimization is an ideal technique for achieving the best cutting parameters combination. To this end, an objective function $F(x)$ is defined and expressed as:

$$DF = \left(\prod_{i=1}^n d_i^{w_i} \right)^{\frac{1}{\sum_{j=1}^n w_j}}, \tag{4.1}$$

$$F(x) = -DF,$$

$$d_i = \begin{cases} 0 & \text{if: } y_i \leq y_{i \min}, \\ y_i - \frac{y_{i \min}}{y_{i \max}} & \text{if: } y_{i \min} \leq y_i \leq y_{i \max}, \\ 1 & \text{if: } y_i \geq y_{i \max}. \end{cases} \tag{4.2}$$

If the objective function is to minimize the output response, then (d_i) will be given as:

$$d_i = \begin{cases} 0 & \text{if: } y_i \leq y_{i \min}, \\ y_{i \max} - \frac{y_i}{y_{i \max}} - y_{i \min} & \text{if: } y_{i \min} \leq y_i \leq y_{i \max}, \\ I & \text{if: } y_i \geq y_{i \max}, \end{cases} \quad (4.3)$$

where (y_i) is the response value, $(y_{i \min})$ and $(y_{i \max})$ representing the minimum and maximum values of the response (i) respectively.

Three optimization operations have been carried out in terms of quality, productivity, and quality-productivity [28-30]. The first procedure consists on finding out the minimum of the surface roughness, while the second seeks the maximum of the material remove rate. The third case is interesting since it combines a high productivity along with a better surface quality. The parameter ranges defined for the optimization processes are summarized in Tab.6.

The results of three optimizations are displayed in Figs 13, 14 and 15. Concerning the surface roughness optimization, the optimal cutting parameters are recorded as: $Vc=654 \text{ m/min}$, $f=0.02 \text{ mm/rev}$ and $ap=0.2 \text{ mm}$ while the optimized surface roughness and the material removal rate are found equal to $Ra=0.40 \mu\text{m}$ and $MRR=2.613 \text{ cm}^3/\text{min}$.

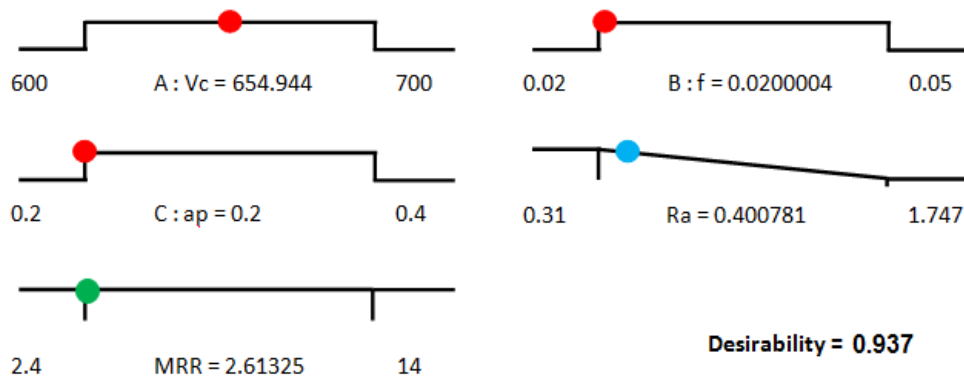


Fig.13. Ramp of desirability function for Ra .

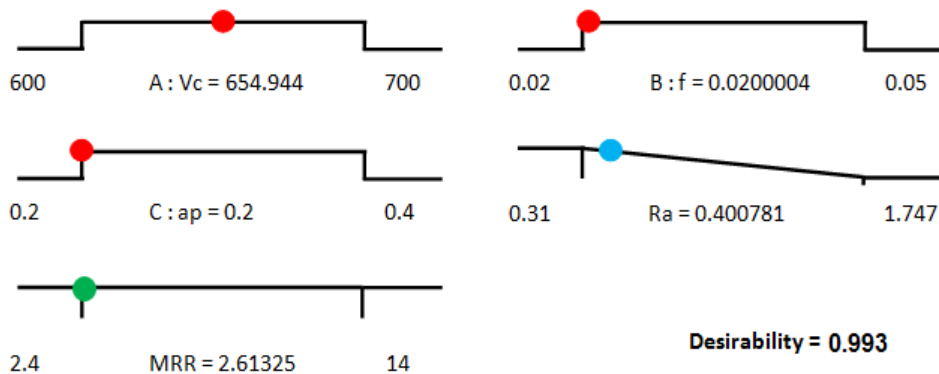


Fig.14. Ramp of desirability function for MRR .

Figure 14 presents the optimal cutting parameters for the material removal rate optimization. They are $V_c=700$ m/min, $f=0.05$ mm/rev, and $ap=0.4$ mm. The optimized material removal rate and surface roughness achieved are $MRR=13.916$ cm³/min and $Ra=0.535$ μm.

Table 6. Goals and parameters ranges when optimizing both quality and productivity.

Name	Goal	Lower limit	Upper limit	Lower weight	Upper weight	Importance		
						Quality	Productivity	Combined
V_c	In range	600	700	1	1	3	3	3
f	In range	0.02	0.05	1	1	3	3	3
ap	In range	0.2	0.4	1	1	3	3	3
Ra	Minimize	0.31	1.747	1	1	5	None	5
MRR	Maximize	2.4	14	1	1	None	5	5

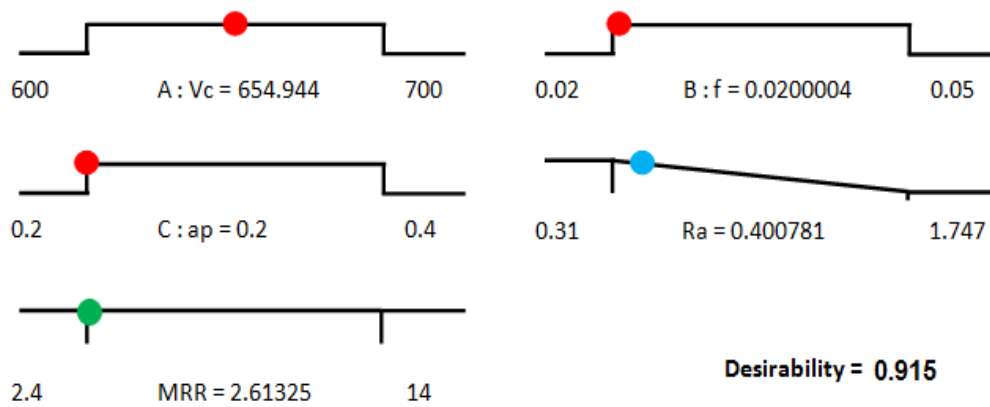
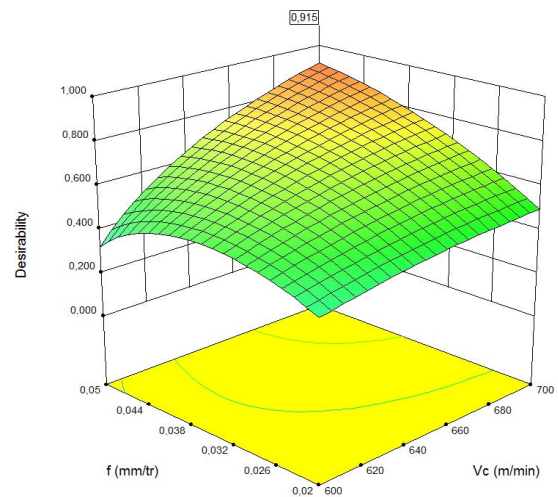
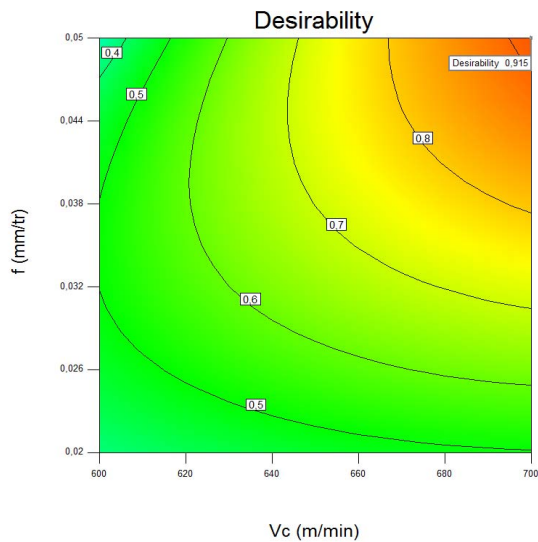


Fig.15. Ramp of combined desirability function.



(a)

(b)

Fig.16. Results of the desirability function: (a) for Ra and (b) MRR .

The last optimization operation concerns a bi-objective optimization pertaining to a better surface finish and higher productivity, and is shown in Fig.15. The cutting speed, feed rate and depth of cut are achieved as 700 m/min , 0.05 mm/rev and 0.4 mm respectively. Furthermore, the optimized surface roughness and material removal rate are found as $Ra=0.535\text{ }\mu\text{m}$ and $MRR=13.91\text{ cm}^3/\text{min}$.

In fact, the optimal cutting parameters have been achieved with a minimum value of (Ra) along with a maximum value of (MRR) when equal weights were set as a desired condition. Moreover, the point displaying the highest desirability is shown in Figs 16(a) and (b), and is represented by: $Vc=700\text{m/min}$, $f=0.05\text{mm/rev}$, and $ap=0.4\text{mm}$. The optimal regions taking the overall desirability value of 0.914 indicate closeness to the target response.

5. Chip formations

The chip shape constitutes a good indicator of the deformation having occurred during the machining process. The chip formation mode depends on the cutting conditions, the workpiece material and the tool geometry. In cutting operations, the chip control plays a major role in checking the quality of the procedure. A mastery of the chip formation contributes to improving the machining process, guaranteeing the geometric quality of the machined surfaces as well as productivity. Thus, chip formation control is one of the key factors in turning aluminum alloy [31-32]. All the chips produced are of continuous type. However, as the speed increases, the chip thickness decreases irrespective of the cutting conditions. Similar explanations have been mentioned in [6] regarding the effect of the cutting speed (Vc) on the chip formation. Chip fracture is also fast at low (Vc), which results in a high (Ra).



Fig.17. Chip breaking.

6. ANN approach

The artificial neural network method is a potentially trustable approach that provides nonlinear complex relationships describing physical aspects of several phenomena [16]. It has numerous advantages among which is the fact that it can truly learn by registering data sets. The *ANN* is a prominent tool used for random function estimation in order to forecast output machining processes. It is potentially accurate and can be used as an alternative to the full-based modeling approach offering the modeling of complex nonlinear relationships.

Within this part of the study, both the surface roughness (Ra) and material removed rate (MRR) are modeled independently according to different targeted architectures. The number of neurons in the input layer is preset as three represented by the cutting speed, the feed rate and the depth of cut. The output layer has a single neuron, that is the target response represented either by (Ra) or (MRR). The activation function used in this research is a hyperbolic tangent ($TanH$) which is a sigmoid function (Eq.6.1) that transforms values between -1 and +1

$$\text{Tan } H = \frac{e^{2x} - 1}{e^{2x} + 1} \quad (6.1)$$

where: (x) represents a linear combination of the (X) variables.

7. RSM and ANN models

In order to assess the fitting and prediction capabilities of the models obtained by the application of the ANN and RSM approaches, coefficients of determination (R^2), concert function error analysis of the root mean square error (RMSE) and mean predictive error (MPE) are used to compare the investigated and forecasted data for (Ra) and (MRR) [33]. The coefficient of determination (R^2), RMSE and MPE are expressed as [34, 36]:

$$R^2 = \frac{\sum_{i=1}^n (y_{i,p} - y_{i,e})}{\sum_{i=1}^n (y_{i,p} - y_{average})^2}, \quad (7.1)$$

$$RMSE = \frac{\sqrt{\sum_{i=1}^n (y_{i,e} - y_{i,p})^2}}{n}, \quad (7.2)$$

$$MPE (\%) = \frac{100}{n} \sum_{i=1}^n \left| \frac{(y_{i,e} - y_{i,p})}{y_{i,p}} \right| \quad (7.3)$$

where (n) is the number of trials, ($y_{i,e}$) the experimentally registered data of the i^{th} test, ($y_{i,p}$) the predicted value of the i^{th} test provided according to the model and ($y_{average}$) is the averaging of the experimentally registered data. In order to compare the RSM and ANN developed models and determine which technique can adequately and precisely visualize the surface roughness and material removed rate, residuals of both approaches are plotted and compared.

7.1. Artificial Neural Networks based-models

In order to suggest an ANN model, an architecture of the neural network should be built, the intention being to acquire an ANN model with optimal size and smallest errors during the testing and validation stages [36]. In this case, a learning rate of 0.01 is set. During this phase, the number of iterations is varied while the screening of the finest number of neurons in the single hidden layer (H) according to the best (R^2), lowest of both (RMSE) and (MPE) is performed.

Figure 18 shows the ANN architecture of the arithmetic mean roughness (Ra) model. The suggested number of iterations regarding this architecture is 1500. It leads to high correlation and low registered errors in terms of RMSE and MPE, and achieves the performance parameters according to the ANN model for training as 0.999 for R^2 , 0.00103 for RMSE and 3.1638% for MPE. Regarding the validation stage, their relevant values are found to be 0.999 for R^2 , 6.661 e-16 for RMSE and 3.1638% for MPE.

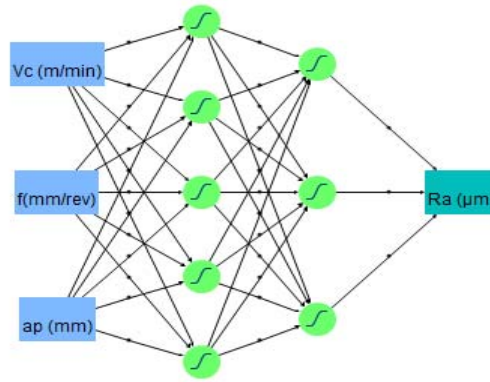


Fig.18. ANN architecture of (*Ra*) model.

7.2. Comparison between *RSM* and ANN models

The present comparison aims at determining which estimating model is capable of achieving results that are the closest possible and fits experimental data. Furthermore, it intends to find out the advantages of each approach and the differences that separate them. Figure 19 displays both *ANN* and *RSM* predicted results along with the experimental ones.

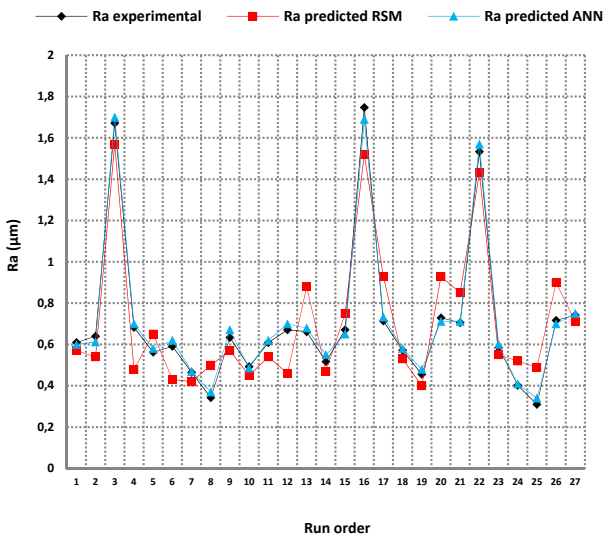


Fig.19. Actual vs predicted values for (*Ra*) model.

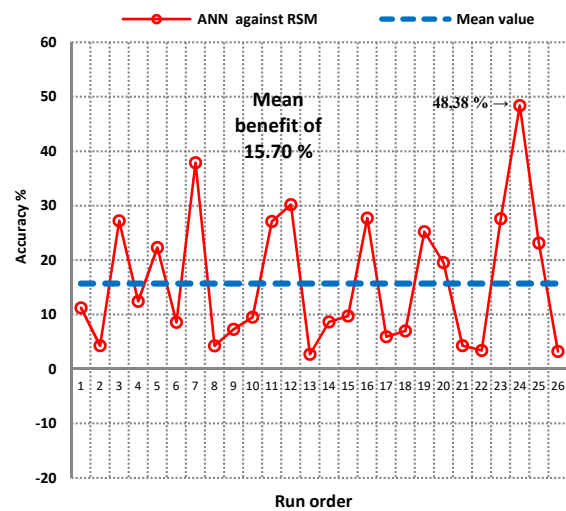


Fig.20. ANN accuracy against *RSM* for (*Ra*) model.

It shows the deviations between the *ANN* predicted results and experimental ones to be less significant than those of its *RSM* counterpart. For the surface roughness, the *RSM* model leads to $R^2=0.8548$ while it achieves $R^2=0.9999$ for the *ANN* model.

Moreover, in terms of the surface roughness the *RSM* model, *RMSE* and *MPE* attain 0.2595 and 18.08 %, respectively, while the application of surface roughness *ANN* model led to 0.00103 and 3.1638 %. Furthermore, for the whole design space, the *ANN* prediction model produces benefits in terms of precision of the order of 48.39 % compared to 15.7% attained by the *RSM* (Fig.20). This leads to a conclusion that *ANN* models exceed those of *MSN* in terms of precision and closeness to experimental data. These results are in perfect agreement with many research works [20,25].

8. Conclusions

In the present study, the analysis of both the surface roughness and the material removal rate in the turning operation of the *EN AW 1350* aluminum alloy by coated carbide tool inserts is presented. On the basis of the results obtained, the following conclusions are drawn:

- The analysis of the machining parameters through the application of the Response Surface Methodology approach allows the exploration of the influence of each factor on the response outputs represented in the present case by the surface roughness (quality) and the material removal rate (productivity).
- It is noticed that the feed rate develops the highest contribution with a contribution of 58.87 % followed by the depth of cut with 34.99 %.
- The statistical analysis (ANOVA) shows that the most influential factors on the evolution of the surface roughness were represented by the cutting speed (V_c) and the feed rate (f) with contributions reaching 38.16% and 28.69% on (Ra) respectively.
- The statistical analysis shows that both models investigated are valid. The correlations coefficients of the quadratic model are respectively 85.50% for the surface roughness and 99.98% for the material removal rate.
- The quadratic response model was optimized using the desirability function approach and achieved an optimum of $Ra=0.535\mu m$ for a desirability of 0.915 for $V_c=700 m/min$, $f=0.05 mm/rev$ and $a_p=0.4 mm$. A minimization of (Ra) and maximization of (MRR) were applied.
- The models developed in this study can be used efficiently in the metal manufacturing industry and would be helpful in selecting the optimum cutting regimes for the optimization of turning aluminum alloys.
- All the chips that were produced were of continuous type. However, the chip thickness decreased with the increase of the speed for all the cutting conditions investigated.
- Within the handled range, the ANN prediction model developed better models for both surface roughness and material removed rate than its RSM counterpart. In terms of (Ra), the RSM achieved a coefficient of determination $R^2=0.8548$, a root mean square error $RMSE=0.02595$ and a mean predictive error $MPE=18.09\%$. The corresponding values achieved by the ANN were $R^2=0.999$, $RMSE=0.00103$ and $MPE=3.1638\%$. Consequently, the ANN prediction model led to a mean benefit of 15.70 % against its RSM prediction counterpart.

Acknowledgments

This work was supported by the General Directorate of Scientific Research and Technological Development (DGRSDT) affiliated to the Algerian Ministry of Higher Education and Scientific Research (MESRS). Fruitful discussions with members of LMC (U. Constantine-1), LMS (U. Guelma), LMANM (U. Guelma) and LR3MI (U. Annaba) laboratories are highly appreciated.

Nomenclature

- ANOVA – analysis of variance
 ANN – artificial neural network
 a_p – depth of cut (mm)
 Adj MS – adjusted mean squares
 DF – degrees of freedom
 V_c – cutting speed (m/min)

f – feed rate (mm / rev)

HV – Vickers hardness

MPE – mean predictive error

MRR – material removal rate (cm^3 / min)

PC% – percentage contribution ratio (%)

R^2 – determination coefficient

Ra – arithmetic average of absolute roughness (μm)

RSM – response surface methodology

$RMSE$ – root mean square error

Seq SS – sequential sum of squares

References

- [1] Kivak T., Samtaş G. and Çiçek A. (2012): *Taguchi method based optimization of drilling parameters in drilling of AISI 316 steel with PVD monolayer and multilayer coated HSS drills.*– Measurement, vol.45, No.6, pp.1547-1557.
- [2] Chen Y., Sun R., Gao Y. and Leopold J. (2017): *A nested-ANN prediction model for surface roughness considering the effects of cutting forces and tool vibration.*–Measurement, vol.98, pp.25-34.
- [3] Mikołajczyk T., Nowicki K., Bustillo A. and Pimenov D.Y. (2018): *Predicting tool life in turning operations using neural networks and image processing.*–Mechanical Systems and Signal Processing, vol.104, pp.503-513.
- [4] Klocke RF., Lortz W. and Trauth D. (2018): *Analysis of the dynamic chip formation process in turning.*– International Journal of Mechanical Sciences, vol.135, pp.313-324.
- [5] Garcia N., Feix E.C., Mendel H.T., Gonzalez A.R. and Souza A.J. (2012): *Optimization of cutting parameters for finish turning of 6082-T6 aluminum alloy under dry and RQL conditions.*– Journal of the Brazilian Society of Mechanical Sciences and Engineering, vol.41, No.8, pp.1-10.
- [6] Bhushan R.K. (2020): *Impact of nose radius and machining parameters on surface roughness, tool wear and tool life during turning of AA7075/SiC composites for green manufacturing.*– Mechanics of Advanced Materials and Modern Processes, vol.6, No.1, pp.1–18.
- [7] Musavi S. H., Sepehrikia M., Davoodi B. and Niknam S.A. (2022): *Performance analysis of developed micro-textured cutting tool in machining aluminum alloy 7075-T6: assessment of tool wear and surface roughness.*–The International Journal of Advanced Manufacturing Technology, vol.119, pp.3343-3362.
- [8] Azimi A., Tutunchilar S., Faraji G. and Besharati Givi M.K. (2012): *Mechanical properties and microstructural evolution during multi-pass ECAR of Al 1100–O alloy.*–Materials and Design, vol.42, pp.388-394.
- [9] Liu Y., Meng G.Z. and Cheng Y.F. (2009): *Electronic structure and pitting behavior of 3003 aluminum alloy passivated under various conditions.*– Electrochimica Acta, vol.54, No.17, pp.4155-4163.
- [10] Fang N., Srinivasa Pai P. and Mosquea S. (2010): *The effect of built-up edge on the cutting vibrations in machining 2024-T351 aluminum alloy.*– Int. J. Adv. Manuf. Technol., vol.49, No.1-4, pp.63-71.
- [11] Demir H. and Gündüz S. (2009): *The effects of aging on machinability of 6061 aluminium alloy.*– Materials and Design, vol.30, No.5, pp.1480-1483.
- [12] Sahoo P., Pratap A. and Bandyopadhyay A. (2017): *Modeling and optimization of surface roughness and tool vibration in CNC turning of Aluminum alloy using hybrid RSM-WPCA methodology.*– International Journal of Industrial Engineering Computations, vol.8, No.3, pp.385-398.
- [13] Bouacha K., Yallese M. A., Mabrouki T. and Rigal J.F. (2010): *Statistical analysis of surface roughness and cutting forces using response surface methodology in hard turning of AISI 52100 bearing steel with CBN tool.*– Int. Journal of Refractory Metals & Hard Materials, vol.28, No.3, pp.349-361.

- [14] Bouacha K., Yallese M. A., Khamel S. and Belhadi S. (2014): *Analysis and optimization of hard turning operation using cubic boron nitride tool.*–Int. Journal of Refractory Metals and Hard Materials, vol.45, pp.160-178.
- [15] Yallese M.A., Boulanouar L. and Chaoui K. (2004): *Usinage de l'acier 100Cr6 trempé par un outil en nitrure de bore cubique.*– Mechanics & Industry, vol.5. No.4, pp.355-368.
- [16] Das B., Roy S., Rai R.N. and Saha S.C. (2015): *Studies on effect of cutting parameters on surface roughness of Al-Cu-TiC MMCs: an artificial neural network approach.*–Procedia Computer Science, vol.45, pp.745-752.
- [17] Palavar O., Özyürek D. and Kalyon A. (2015): *Artificial neural network prediction of aging effects on the wear behavior of IN706 superalloy.*–Materials & Design, vol.82, pp.164-172.
- [18] Tebassi H., Yallese M., Khettabi R., Belhadi S., Meddour I. and Girardin F. (2016): *Multi-objective optimization of surface roughness, cutting forces, productivity and power consumption when turning of Inconel 718.*– International Journal of Industrial Engineering Computations, vol.7, No.1, pp.111-134.
- [19] Chabbi A., Yallese M. A., Meddour I., Nouioua M., Mabrouki T. and Girardin F. (2017): *Predictive modeling and multi-response optimization of technological parameters in turning of Polyoxymethylene polymer (POM C) using RSM and desirability function.*– Measurement, vol.95, pp.99-115.
- [20] Chabbi A., Yallese M.A., Nouioua M., Meddour I., Mabrouki T. and Girardin F. (2017): *Modeling and optimization of turning process parameters during the cutting of polymer (POM C) based on RSM, ANN, and DF methods.*– The International Journal of Advanced Manufacturing Technology, vol.91, No.5-8, pp.2267-2290.
- [21] Mobin M., Mousavi S. M., Komaki M. and Taviana M.A. (2018): *Hybrid desirability function approach for tuning parameters in evolutionary optimization algorithms.*–Measurement, vol.114, pp.417-427.
- [22] AL-Refaie A., AL-Alaween W., Diabat A. and Li M.-H. (2017): *Solving dynamic systems with multi-responses by integrating desirability function and data envelopment analysis.*–J. Intell. Manuf, vol.28, No.2, pp.387-403.
- [23] Kumar N. and Das D. (2016): *Alkali treatment on nettle fibers part II: design of experiment and desirability function approach to study enhancement of tensile properties.*– The Journal of the Textile Institute, vol.108, No.8, pp.1468-1475.
- [24] Das R., Ball A.K. and Roy S.S. (2017): *Optimization of E-jet based micro-manufacturing process using desirability function analysis.*–Industry Interactive Innovations in Science, Engineering and Technology, vol.11, pp.477-484.
- [25] Tebassi H., Yallese M.A., Meddour I., Girardin F. and Mabrouki T. (2016): *On the modeling of surface roughness and cutting force when turning of Inconel 718 using artificial neural network and response surface methodology: accuracy and benefit.*– Periodica Polytechnica Mechanical Engineering, vol.61, No.1, pp.1-11.
- [26] Fnides M., Yallese M. A., Khattabi R., Mabrouki T. and Girardin F. (2017): *Modeling and optimization of surface roughness and productivity thru RSM in face milling of AISI 1040 steel using coated carbide inserts.*– International Journal of Industrial Engineering Computations, vol.8, No.4, pp.493-512.
- [27] Bouzid L., Berkani S., Yallese M. A., Girardin F. and Mabrouki T. (2018): *Estimation and optimization of flank wear and tool lifespan in finish turning of AISI 304 stainless steel using desirability function approach.*– International Journal of Industrial Engineering Computations, vol.9, No.3, pp.349-368.
- [28] Tebassi H., Yallese M., Belhadi S., Girardin F. and Mabrouki T. (2017): *Quality-productivity decision making when turning of Inconel 718 aerospace alloy: a response surface methodology approach.*–International Journal of Industrial Engineering Computations, vol.8, No.3, pp.347-362.
- [29] Ben Fathallah B., Saidi R., Dakhli C., Belhadi S. and Yallese M. A. (2019): *Mathematical modelling and optimization of surface quality and productivity in turning process of AISI 12L14 free-cutting steel.*– International Journal of Industrial Engineering Computations, vol.10, No.4, pp.557-576.
- [30] Saidi R., Fathallah B. B., Mabrouki T., Belhadi S. and Yallese M. A. (2019): *Modeling and optimization of the turning parameters of cobalt alloy (Stellite 6) based on RSM and desirability function.*– The International Journal of Advanced Manufacturing Technology, vol.100, No.9-12, pp.2945-2968.
- [31] Vilches F. J. T., Hurtado L. S., Fernández F.M. and Gamboa C. B. (2017): *Analysis of the chip geometry in dry machining of aeronautical aluminum alloys.*– Applied Sciences, vol.7, No.2, pp.132.
- [32] Jomaa W., Mechri O., Levesque J., Songmene V., Bocher P. and Gakwaya A. (2017): *Finite element simulation and analysis of serrated chip formation during high-speed machining of AA7075-T651 alloy.*–Journal of Manufacturing Processes, vol.26, pp.446-458.
- [33] Ramezani M. (2015): *Surface roughness prediction of particulate composites using artificial neural networks in turning operation.*– Decision Science Letters, vol.4, No.3, pp.419-424.

- [34] Rajendra M., Jena P.C. and Raheman H. (2009): *Prediction of optimized pretreatment process parameters for biodiesel production using ANN and GA.*–Fuel, vol.88, No.5, pp.868-875.
- [35] García-Gimeno R.M., Hervas-Martinez C., Rodriguez-Perez R. and Zurera-Cosano G. (2005): *Modelling the growth of Leuconostocmesenteroides by artificial neural networks.*–International Journal of Food Microbiology, vol.105, No.3, 317-332.
- [36] Kashyzadeh K.R. and Maleki E. (2017): *Experimental investigation and artificial neural network modeling of warm galvanization and hardened chromium coatings thickness effects on fatigue life of AISI 1045 carbon steel.*– J. Fail. Anal. Prev., vol.17, No.6, pp.1276-1287.

Received: January 22, 2022

Revised: March 28, 2022